

Dedicated to the memory of V.L. Indenbom

# Grain Boundary Faceting—Roughening in Zn

B. B. Straumal, A. S. Gornakova, and V. G. Sursaeva

Institute of Solid State Physics, Russian Academy of Sciences, Chernogolovka, Moscow oblast, 142432 Russia

e-mail: straumal@issp.ac.ru

Received May 27, 2009

**Abstract**—The change in the grain-boundary (GB) shape with an increase in temperature near the GB faceting—roughening phase transition has been studied. The GB facet length decreases with an increase in temperature to complete facet disappearance. The facet orientation is determined by the constrained coincidence site lattice (CCSL). Facets are located along close-packed CCSL planes. Above the roughening temperature  $T_R$ , the tangents to the faceted and rough GB portions at the point of emergence of the first-order ridge are located along the close-packed CCSL planes (as facets below  $T_R$ ). The faceting—roughening phase transition is reversible. The presence of temperature hysteresis is indicative of first-order phase transition.

PACS numbers: 68.35.-p, 68.35.Rh, 68.35.Ct

DOI: 10.1134/S1063774509060236

## INTRODUCTION

The nature of the formation of the equilibrium-faceted free surface of crystals during their growth or dissolution was analyzed for the first time by Wulff (Professor at Warsaw University and then Kazan University) at the end of the XIX century [1, 2]. In the 1950s, Landau described the role of step formation on flat crystal faces for equilibrium faceting [3]. It was shown by Burton and Cabrera and then by Chernov that the formation of steps on a flat surface at nonzero temperature increases the surface configuration entropy and, therefore, decreases the surface free energy [4–6]. With an increase in the temperature, the equilibrium step concentration increases and becomes infinite at a certain temperature. As a result the flat face completely loses stability (the so-called faceting—roughening phase transition occurs). These phase transitions were analyzed in detail in a number of theoretical and experimental studies [7–13]. In addition, it has been known since Wulff's studies that the outer crystal surface can be divided into a system of flat facets if the total energy of the latter is lower than the energy of the initial surface (despite the fact that this process increases the total surface area). This transformation is referred to as the faceting phase transition.

In recent years there has been renewed interest in the faceting phase transitions on the free surface [14–20]. One reason is that faceted surfaces contain a very regular equilibrium 1D set of steps or a 2D array of pyramids. Such faceted surfaces can be used, for example, as substrates for fabricating quantum wires

or quantum dots; i.e., they are promising for nano-electronic applications [21].

Grain boundaries (GBs) can also be faceted. Faceting of GBs indicates that they are special. The reason for this is that, if misorientations coincide, the lattices of two grains form a general superlattice—the so-called coincidence site lattice (CSL). The most pronounced GB facets lie in close-packed CSL planes [22, 23]. In this case, the role of close-packed CSL planes for GBs is similar to that of close-packed lattice planes for crystal free-surface faceting. The numerous and interesting phase transitions on free surfaces, which are related to the occurrence and disappearance of crystal faceting and to the dependence of the faceting phase transition on the outer surface orientation, should have analogs on GBs [24–28]. In particular, it was shown by Balluffi [29] that facets on GBs in aluminum and gold reversibly disappear with an increase in temperature and its approach to the melting point. This fact indicates that faceting—roughening phase transitions may occur on GBs. The features of the behavior of tilt boundaries in copper near the coincidence misorientation  $\Sigma$  ( $\Sigma$  is the ratio of the number of lattice sites per grain to the number of coincident sites) were explained in terms of the faceting—roughening phase transition at GBs [30].

With an increase in the parameter  $\Sigma$ , the CSL energy relief becomes shallower. As a result, an increase in  $\Sigma$  reduces the lower temperature limit at which thermal disordering leads to the disappearance of the special structures and properties at boundaries. In principle, if one considers GBs with different orientations in a CSL with fixed  $\Sigma$ , the energy relief at the boundary should also depend on the density of coincident sites lying in a given CSL plane. In other words,

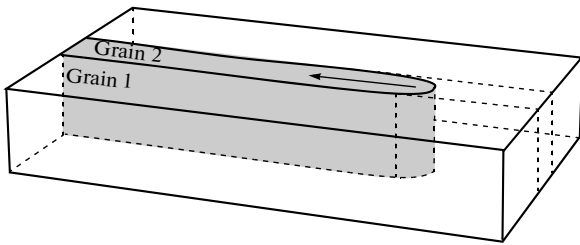


**Fig. 1.** Schematic diagram of a bicrystal sample for studying the migration and faceting of a single GB at a constant (capillary) driving force.

the smaller the density of coincident sites and the higher the indices of a given CSL plane, the shallower the CSL-induced energy relief should be. One might expect an increase in the number of equilibrium faces in equilibrium faceting of special GBs at fixed  $\Sigma$  with a decrease in temperature; this situation was observed on GBs  $\Sigma 3$  and  $\Sigma 9$  in copper [31]. In addition to the planes with low CSL indices, CSL faces with constantly increasing indices will arise in this case.

In this paper, we review the results obtained by studying the faceting—roughening transition in zinc—a material with a hexagonal close-packed (hcp) lattice.

## EXPERIMENTAL

Flat zinc single crystals, bicrystals, and tricrystals with a  $(11\bar{2}0)$   $(10\bar{1}0)$  surface were grown by the modified Bridgeman method from zinc of 99.999 wt % purity grade [32–34]. Some elongated twin plates of very homogeneous width over the entire length were obtained by the weak deformation of these  $(11\bar{2}0)$  single crystals. The twin plates obtained are oriented perpendicularly to the surface and have the same width

over the entire length. The axes  $[11\bar{2}0]$  in both grains are also perpendicular to the sample surface. Such twin-boundary geometry is characteristic of most metals with a hcp lattice [35]. The parallel elongated sides of a twin plate are formed by coherent symmetric twin GBs (STGBs)  $(1\bar{1}02)_1/(1\bar{1}0\bar{2})_2$ . In addition, we grew bicrystals with tilt boundaries  $[10\bar{1}0]$  having misorientation angles  $\theta = 30^\circ$  and  $84^\circ$  and a tricrystal  $[10\bar{1}0]$  with three tilt boundaries having misorientation angles of  $43^\circ$ ,  $37^\circ$ , and  $6^\circ$ .

Since zinc is optically anisotropic, the GB shape in it can be studied in polarized light. The steady-state shape of a slowly migrating asymmetric twin GB located at the end of a twin plate and the shapes of the migrating part of a GB half-loop or triple junction (Fig. 1) were studied directly in a hot stage for a light microscope in the range of 590–692 K. The samples were placed in pure nitrogen to avoid oxidation. The GB shape was fixed in the experiment by a video camera connected to a microscope and video recorder. This method was initially developed for studying the GB migration [32–34, 36, 37]. The driving force for changing the GB shape, which is related to GB phase transitions, is generally insufficient for changing the GB shape over any reasonable time. Therefore, a constant capillary driving force was used to cause GB migration. In other words, a GB migrates with a simultaneous reduction of its length and, therefore, a decrease in the free energy of the system. Thus, the GB migration was caused by a constant capillary driving force in our experiments. During slow displacement induced by a capillary driving force, a GB can acquire an equilibrium shape which corresponds to the temperature of the experiment. This method was used, for example, in our experimental studies of the special GB—general GB phase transitions [38–47].

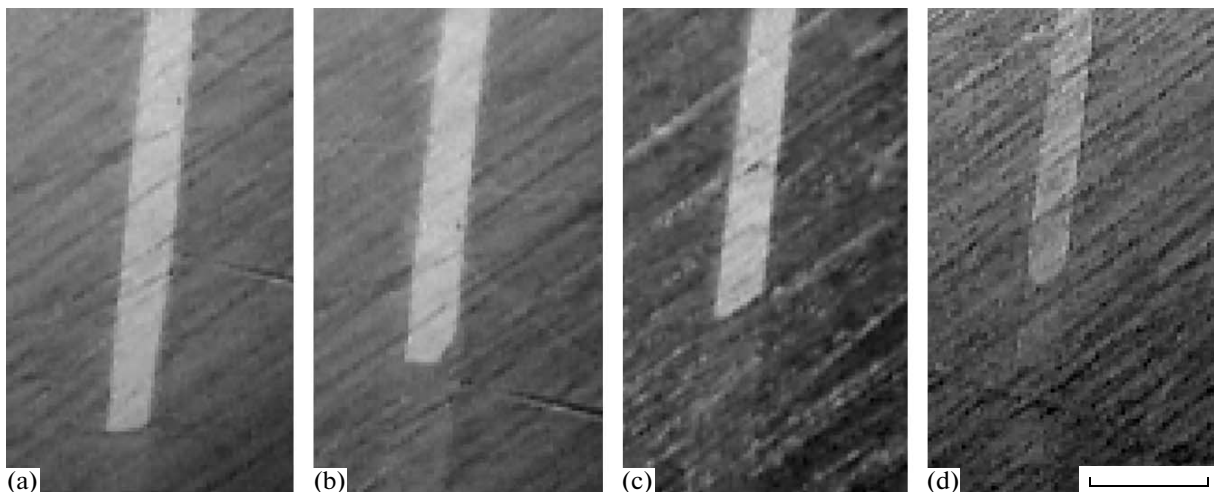


**Fig. 2.** Shape of twin plates in a flat zinc  $[11\bar{2}0]$  single crystal at temperatures of (a) 632, (b) 652, (c) 682, and (d) 692 K. The scale ruler length is 100  $\mu\text{m}$ .

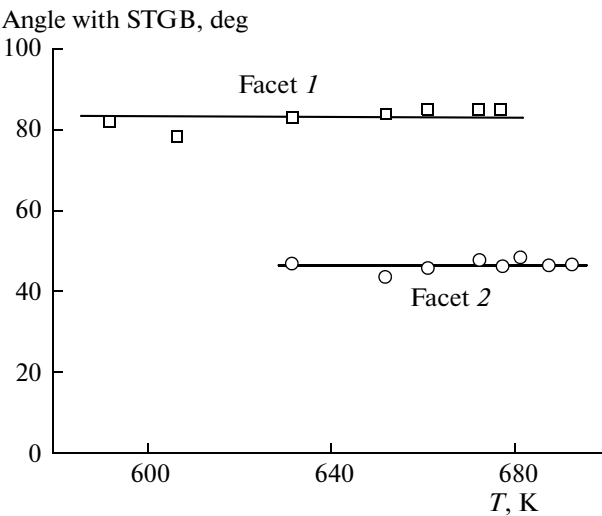


**Fig. 3.** Angle between the STGB and facets formed at the end of twin plates in flat zinc  $[1\bar{1}\bar{2}0]$  single crystals at different temperatures. Circles and squares denote the  $(110)_{\text{CSL}}$  and  $(010)_{\text{CSL}}$  facets on twin plates.

## RESULTS AND DISCUSSION

We chose zinc to study because it has a noncubic lattice and is, therefore, optically anisotropic. As a result, the GB shape in zinc can be studied directly in the hot stage of a light microscope in polarized light. One drawback of the zinc noncubic lattice is that the ratio of the periods  $a$  and  $c$  of the hexagonal lattice is irrational; therefore, simple CSLs cannot be constructed for GBs in zinc. Hence, it is necessary to use the method of constrained coincidence site lattices (CCSLs) [48, 49].

### *Twin Boundaries: Replacing One Facet with Another*

We began our analysis of GB faceting in zinc with the simplest case of twin boundaries. It was shown in studies on copper that twin boundaries  $\Sigma 3$  in cubic metals are very good objects for studying faceting [31, 50]. For example, the ends of twin plates in copper exhibited various  $\Sigma 3$  CSL facets, such as  $(010)_{\Sigma 3\text{CSL}}$  and  $(110)_{\Sigma 3\text{CSL}}$ , as well as the  $82^{\circ}9R$  facet, which does not belong to the CSL [31, 50].

The micrographs in Fig. 2 show the change in the GB shape at the twin plate vertex in zinc upon heating. The GB shape at the twin plate vertex significantly differs from the curved shape of the GB half-loop in zinc bicrystals containing general GBs [32, 34, 37]. At low temperatures the twin vertex consists of one flat facet 1 oriented almost perpendicularly to the STGB (Fig. 2a). An increase in temperature leads to the formation of the second facet 2 (Fig. 2b). Facet 2 has an angle of about  $45^{\circ}$  with both STGB and facet 1. Upon further heating, facet 2 is elongated and facet 1 is shortened. Above some temperature, only facet 2

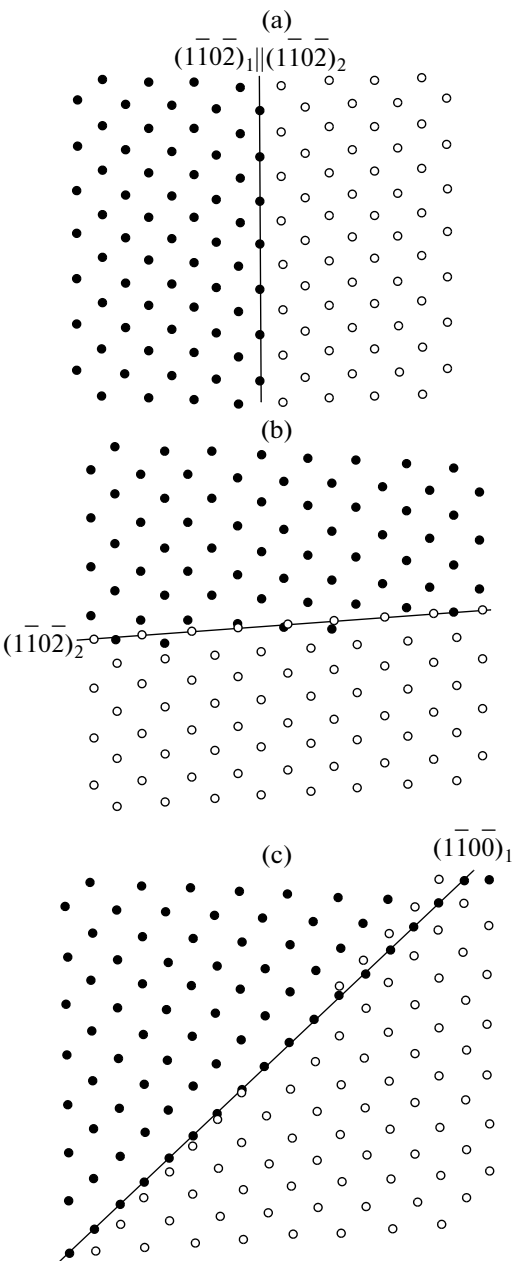


**Fig. 4.** Crystallographic features of the facets observed: (a)  $(1\bar{1}0\bar{2})_1/(1\bar{1}0\bar{2})_2$  STGB, (b) facet 1 is almost parallel to the  $(1\bar{1}0\bar{2})_2$  plane and makes an angle of  $84^{\circ}$  with the STGB, and (c) facet 2 is almost parallel to the  $(1\bar{1}00)_1$  plane and makes an angle of  $46^{\circ}$  with the STGB.

remains at the twin vertex, which is an acute angle with the STGB (Fig. 2c). At temperatures close to the zinc melting point, the ridges (facet intersection lines) become curved; however, the flat portion of facet 2 is still observed (Fig. 2d). Figure 3 shows the temperature dependences of the angles between STGB and facets 1 and 2. The average values of the angles for facet 1 and 2 are  $84^{\circ}$  and  $46^{\circ}$ , respectively. Below 622 K the twin plate vertex contains only facet 1.

Between 622 and 677 K, facets 1 and 2 coexist. Above 677 K, there is only facet 2. The schematic diagrams in Fig. 4 show the CSL and crystallography of the facets observed. The symmetric twin GB is coherent and coincides with  $(1\bar{1}0\bar{2})$  planes in both lattices (Fig. 4a). Facet 1 is almost parallel to the  $(1\bar{1}0\bar{2})_2$  plane, while the coincidence in this case is much worse than for the coherent STGB (Fig. 4b). Facet 2 is almost parallel to the  $(1\bar{1}00)_1$  plane (Fig. 4c). Figure 5 shows the temperature dependence of the normalized lengths  $A_1$  and  $A_2$  of the facets.  $A_1$  monotonically decreases from 1 at 607 K to 0 at 682 K, whereas  $A_2$  increases from 0 at 607 K, reaches a maximum (0.95) at 682 K, and then decreases to 0.58 at 692 K. The length  $A_2$  decreases in the absence of other facets. Above 692 K the twin plate end becomes curved. The disappearance of sharp ridges at the intersection of GB facets can be explained by the roughening of GB facets when they approach the melting point. Figure 6 shows the phase diagram for faceting twin boundaries in zinc. One can distinguish three GB phase transitions:

- facet 1 disappears between 677 and 682 K;
- facet 2 arises between 607 and 677 K;
- roughening begins and an unfaceted GB phase arises between 682 and 692 K.

STGB is stable at all temperatures. Figure 7 shows schematic Wulff diagrams, which illustrate the possible energy factors responsible for the GB faceting and roughening of facet 2. The energy minimum for STGB occurs at all temperatures. At 593 K there are minima for both facets, 1 and 2; however, facet 2 is metastable. At 653 K both facets are stable and present in the equilibrium GB shape. At 683 K the roughening phase transition begins, the energy minimum for facet 1 disappears, and only facet 2 remains stable, manifesting itself in the equilibrium GB shape. At 688 K the roughening continues, the energy minima of both remaining facets become shallower, and the curved part of the GB loop successively absorbs flat portions of facets.

Our study of the twin GB shape allowed us to observe for the first time the GB faceting phase transition, when one smooth facet is replaced with another [51]. Previously only two types of GB faceting phase transitions were observed:

(i) Reversible GB faceting—roughening phase transition with an increase in temperature and dissociation of smooth unfaceted GB into facets alongside a decrease in temperature in aluminum and gold [29, 52].

(ii) Dissociation of the initial flat GB into flat facets with energies lower than that of the initial boundary [24–28, 53].

Facets on GBs can be observed only near coincidence misorientations. It was shown in [38–47] that GBs have a special structure and properties in a limited range of temperatures and misorientations  $\theta$  near

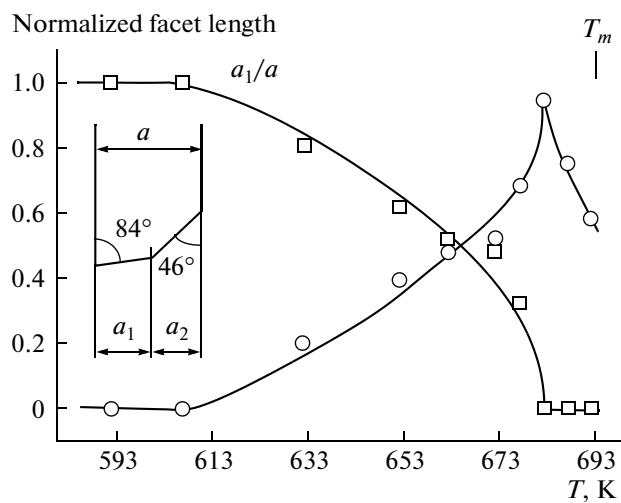


Fig. 5. Temperature dependence of the normalized length of facet 1 ( $84^\circ$ ,  $a_1/a$ , squares) and facet 2 ( $46^\circ$ ,  $a_2/a$ , circles) of twin plates in flat zinc single crystals [1120].

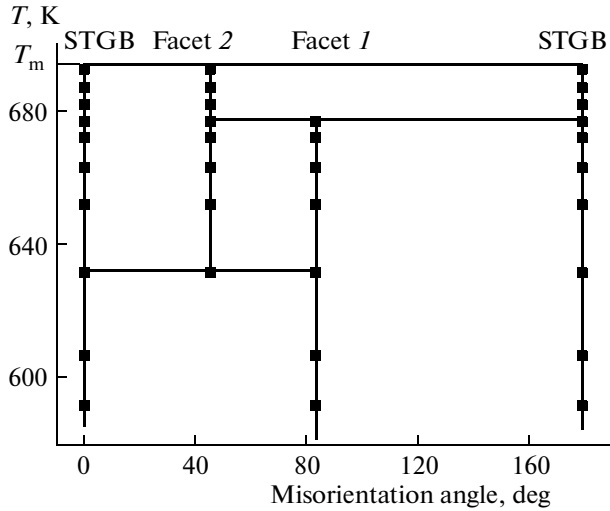
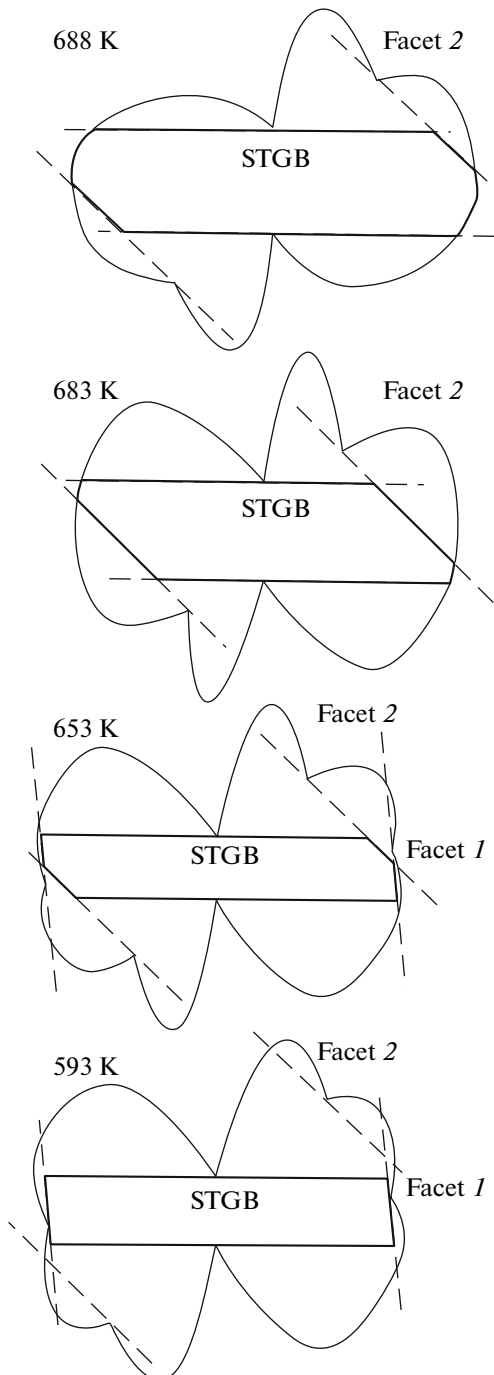


Fig. 6. Phase diagram of different facets on twins in zinc ( $T_m$  is the melting temperature). The facet orientation is shown in the top part of the diagram. Squares denote the experimentally observed facets. The vertical lines indicate the temperature range of stability of the corresponding GB facets. The horizontal lines indicate the upper and lower stability limits of facets 1 ( $84^\circ$ ) and 2 ( $46^\circ$ ).

the coincidence misorientation  $\Theta_\Sigma$ . In other words, an increase in either  $\Delta\theta = |\theta - \Theta_\Sigma|$  or/and temperature leads to the special GB-general GB phase transition and the GB loses its special structure and properties. In particular, this phase transition leads to the disappearance of GB facets. The ratio of the lattice periods  $a$  and  $c$  in zinc is irrational and depends on the temperature. In this context, direct special GB 1—special GB 2 transitions may occur in zinc with a change in temperature and misorientation angle [48, 49]. Therefore, the unusual  $84^\circ$ — $46^\circ$  faceting transition on twin GBs in



**Fig. 7.** Schematic Wulff diagrams for twin plates in flat zinc  $[11\bar{2}0]$  single crystals at different temperatures (593, 653, 683, and 688 K).

zinc can be caused by the transformation from a special  $\Sigma 15a$  GB into the other special  $\Sigma 28a$  GB or from  $\Sigma 28a$  into  $\Sigma 13a$  with an increase in temperature [48, 49]. A similar transformation could cause the kinks in the Arrhenius temperature dependences of GB sliding at tilt boundaries  $\langle 10\bar{1}0 \rangle$  in zinc near the coincidence misorientation  $\Sigma 9$  observed in [54].

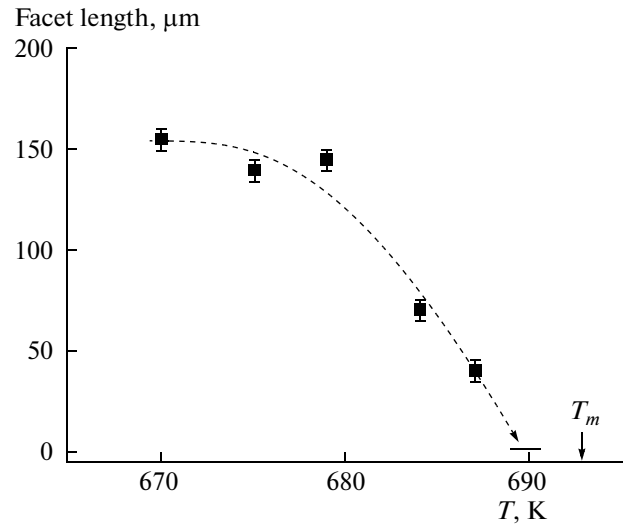


**Fig. 8.** Temperature dependences of the facet length for a triple junction with  $[10\bar{1}0]$  tilt boundaries having misorientation angles  $\theta = 43^\circ, 37^\circ$ , and  $6^\circ$ .

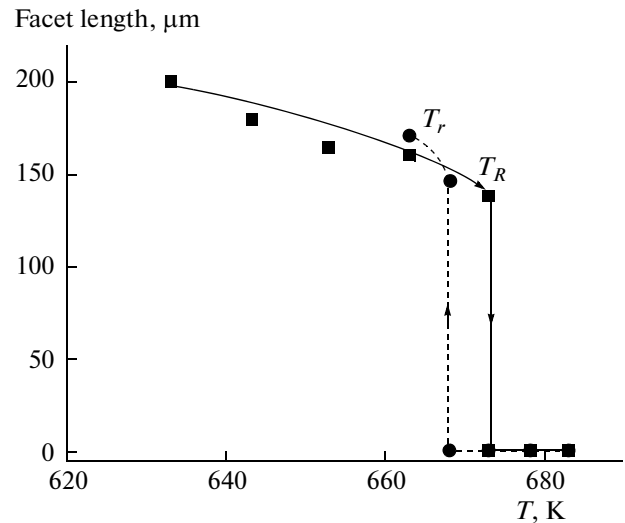


**Fig. 9.** Temperature dependence of the facet length for a  $[10\bar{1}0]$  tilt boundary with the misorientation angle  $\theta = 30^\circ$  upon (squares) heating and (circles) cooling.

### Reversible Roughening upon Heating

The faceting–roughening transition at a migrating GB was experimentally observed for the first time for a triple junction [55]. This junction was formed by three tilt boundaries  $[10\bar{1}0]$  with misorientation angles  $\theta$  of  $43^\circ, 37^\circ$ , and  $6^\circ$ . The investigations were performed in the temperature range  $670$ – $688$  K. The facet length was found to decrease upon heating, and a roughening transition was observed near the zinc melting temperature  $T_m = 692.6$  K; i.e., the facet disappeared (Fig. 8). Subsequent studies were carried out on bicrystals to

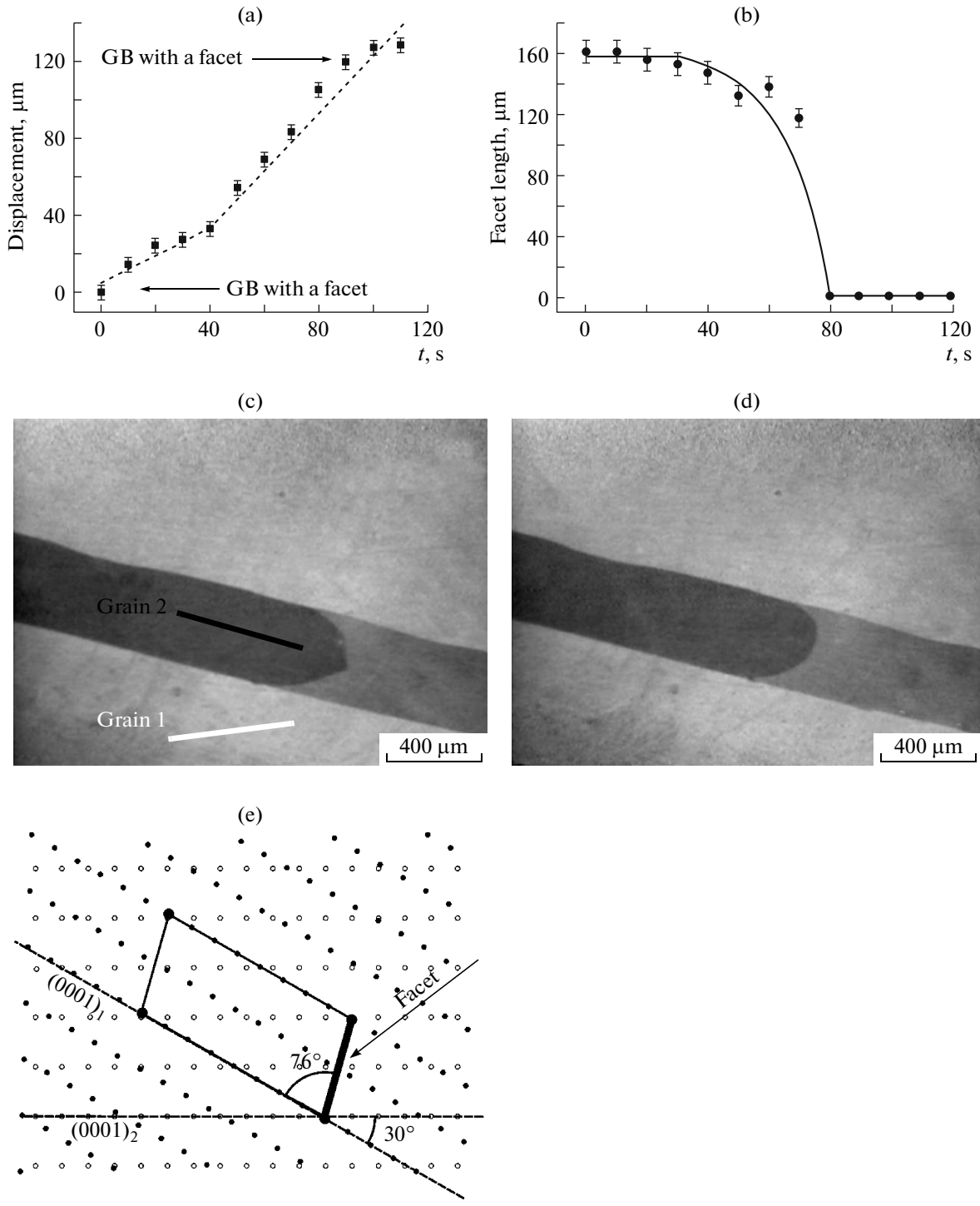


**Fig. 10.** Time dependences of the facet (a) displacement and (b) length, corresponding to a roughening temperature of 673 K, the optical micrographs of a migrating GB (c) with and (d) without a facet, and (e) the CCSL for this boundary.

exclude the effect of the third GB [56]. Figure 9 shows the temperature dependence of the facet length for the tilt boundary  $[10\bar{1}0]$  with the misorientation angle  $\theta = 30^\circ$ . The bicrystal was heated from 630 to 683 K, and a roughening transition was observed at 673 K.

Below and above  $T_R = 673$  K, the migrating GB contained and lacked a facet, respectively. When the sample heated to 683 K began to cool, a reverse faceting transition occurred at  $T_r = 667$  K. Above  $T_r = 667$  K the migrating GB has no facet and below this temper-

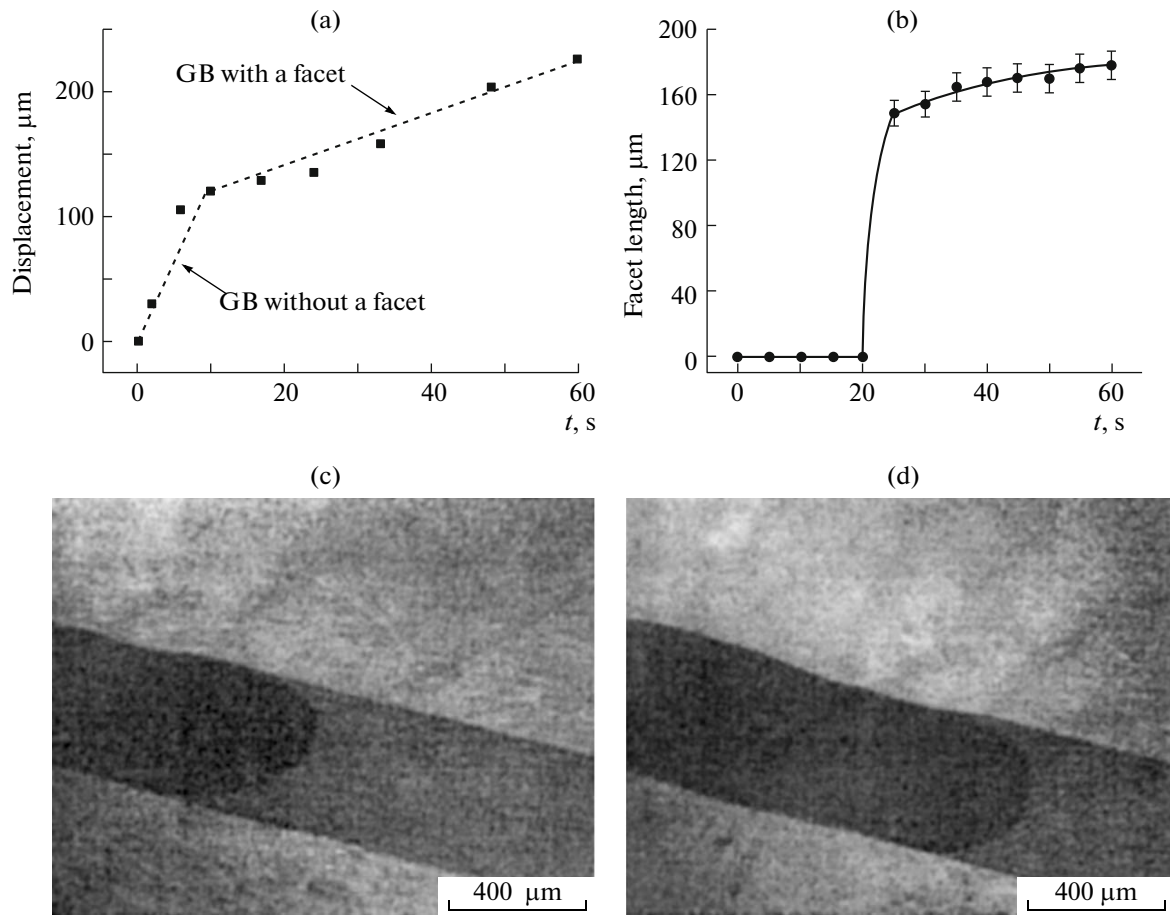


**Fig. 11.** Time dependences of the facet (a) displacement and (b) length, corresponding to a faceting temperature of 668 K and the optical micrographs of a migrating GB (d) with and (c) without a facet.

ature it has. In other words, the reversible faceting—roughening transition at a migrating GB was experimentally found for the first time in zinc.

Figure 10a shows the time dependence of GB displacement. This dependence contains two linear portions with different migration rates. When comparing the time dependences of the GB displacement and facet length (Fig. 10b), one can easily see a correlation between these parameters. The first portion (from 0 to 40 s) in the time dependence of displacement corresponds to the migration of a GB with a facet. Figure 10c shows an optical micrograph for this time interval. The second linear portion (from 40 to 120 s) in the time dependence of the displacement corresponds to the migration of a GB without a facet. The optical micrograph for this time interval is shown in Fig. 10d. It should be emphasized that the facet does not disappear immediately. Below the roughening temperature, there are two phases in the GB: faceted (with a facet) and unfaceted (with curved portions). Above the roughening temperature, there is only one phase in the GB in equilibrium—an unfaceted one. An interesting analogy arises: as in the case of bulk phases, at the transition from the two-phase region of

the phase diagram into the single-phase region (with an increase in temperature), the second-phase particles are dissolved in the matrix not instantaneously but with at a finite rate.

Let us now consider a faceting temperature of 668 K. In this case, the situation is opposite of that observed for roughening. The time dependence of the GB displacement (Fig. 11a) contains two linear portions. The first portion (from 0 to 10 s) corresponds to the migration of a GB without a facet, whereas in the time dependence of the facet length (Fig. 11b) the facet arises only 20 s after. This time interval corresponds to the optical micrograph in Fig. 11c. The second linear portion (from 10 to 60 s) in the time dependence of the GB displacement is related to the migration of a GB with a facet. This time interval corresponds to the optical micrograph in Fig. 11d. In other words, the facet reaches a steady-state length not immediately after a change in the sample temperature but with some delay.

Here, the analogy with the bulk phases can be extended. Upon a transition from the single-phase region of the phase diagram to the two-phase region

(upon cooling), the second-phase particles are formed in the matrix not instantaneously but at finite rate. They require some time to be formed and grow (to reach the volume fraction of the second phase, whose value is determined by the lever rule for bulk phase diagrams). The situation on GBs is the same: with an increase in temperature above  $T_R$ , a facet is dissolved in the unfaceted phase not immediately but after some delay.

## CONCLUSIONS

A systematic in situ study of GB faceting and roughening features was performed for the first time.

The change in the GB shape with an increase in temperature near the GB faceting—roughening phase transition was studied. It was found that one facet is replaced with another at twin boundaries upon heating, which was not observed in materials with a cubic lattice.

The GB facet length decreases with an increase in temperature, and the facet finally disappears.

The kinetics of facet disappearance above the roughening temperature  $T_R$  and the kinetics of the facet formation and growth below the faceting temperature  $T_f$  were investigated.

The facet orientation is determined by the CCSL. Facets are arranged along close-packed CCSL planes. Above  $T_R$  the tangent to the faceted and rough GB portions at the point of first-order ridge emergence are arranged along close-packed CCSL planes (as facets below  $T_R$ ).

A reversible faceting—roughening transition was observed on a migrating GB. The presence of temperature hysteresis is indicative of the first-order phase transition.

## ACKNOWLEDGMENTS

We are grateful to L.S. Shvindlerman, A.L. Petelin, and E.I. Rabkin for their detailed discussion of the results. This study was supported by the Russian Foundation for Basic Research, project nos. 09-02-00294, 09-02-91339-NNIO, 08-08-90105, and 09-03-92481, and the Japanese Society for the Promotion of Science (JSPS S-08191).

## REFERENCES

1. G. V. Wulff, Tr. Varshavsk. Obshch. Estestvoisp. **6**, 7 (1894–1895) [in Russian].
2. G. V. Wulff, Izv. Varshavsk. Un-Ta **7–9** (1895), **1–2**, 1, (1895) [in Russian].
3. L. D. Landau, in *Collected Works Dedicated to the 70th Birthday of Academician A. F. Landau* (Izd-vo Akad. Nauk SSSR, Moscow, 1950), p. 44 [in Russian].
4. W. K. Burton and N. Cabrera, Disc. Faraday Soc. **5**, 33 (1949).
5. W. K. Burton, N. Cabrera, and F. C. Frank, Philos. Trans. R. Soc. London, Ser. A **243**, 299 (1951).
6. A. A. Chernov, Usp. Fiz. Nauk **73**, 277 (1961) [in Russian].
7. A. F. Andreev, Zh. Eksp. Teor. Fiz. **80**, 2042 (1981) [Sov. Phys. JETP **53**, 1063 (1981)].
8. V. I. Marchenko, Zh. Eksp. Teor. Fiz. **81**, 1141 (1981) [Sov. Phys. JETP **54**, 605 (1981)].
9. S. T. Cui and J. D. Weeks, Phys. Rev. Lett. **40**, 733 (1978).
10. J. B. Maxson, D. E. Savage, F. Liu, et al., Phys. Rev. Lett. **85**, 2152 (2000).
11. A. Landa, H. Häkkinen, R. N. Barnett, et al., J. Non-Cryst. Solids **205–207**, 767 (1996).
12. P. A. Gravil and S. Holloway, Phys. Rev. B **53**, 11 128 (1996).
13. H. J. W. Zandvliet, Phys. Rev. B **61**, 9972 (2000).
14. V. E. Fradkov and L. S. Shvindlerman, Fiz. Met. Metalloved. **48**, 297 (1979) [in Russian].
15. M. Yoon, S. G. J. Mochrie, D. M. Zehner, et al., Phys. Rev. B **49**, 16 702 (1994).
16. G. M. Watson, D. Gibbs, D. M. Zehner, et al., Phys. Rev. Lett. **71**, 3166 (1994).
17. S. Song and S. G. J. Mochrie, Phys. Rev. Lett. **73**, 995 (1994).
18. S. Song and S. G. J. Mochrie, Phys. Rev. B **51**, 10 068 (1995).
19. S. Song, M. Yoon, and S. G. J. Mochrie, Surf. Sci. **334**, 153 (1995).
20. M. Yoon, S. G. J. Mochrie, M. W. Tate, et al., Surf. Sci. **411**, 70 (1998).
21. W. W. Mullins and R. F. Sekerka, J. Phys. Chem. Solids **23**, 801 (1962).
22. V. E. Fradkov and L. S. Shvindlerman, Poverkhnost: Fiz., Khim., Mekh., No. 11, 50 (1982) [in Russian].
23. V. M. Kosevich and B. M. Baizul'din, Fiz. Met. Metalloved. **48**, 442 (1979) [in Russian].
24. T. Muschik, W. Laub, M. W. Finnis, and W. Gust, Z. Metallkd. **84**, 596 (1993).
25. W. Laub, A. Oswald, T. Muschik, et al., *Solid–Solid Phase Transformations*, Ed. by W. C. Johnson et al. (Miner. Met. Mater. Soc., Warrendale, 1994), p. 1115.
26. T. Muschik, W. Laub, U. Wolf, et al., Acta Metall. Mater. **41**, 2163 (1993).
27. A. Oswald, W. Laub, W. Gust, and R. A. Fournelle, *Solid–Solid Phase Transformations*, Ed. by W. C. Johnson et al. (Miner. Met. Mater. Soc., Warrendale, 1994), p. 1121.
28. A. Barg, E. Rabkin, and W. Gust, Acta Metall. Mater. **43**, 4067 (1995).
29. T. E. Hsieh and R. W. Balluffi, Acta Metall. **37**, 2133 (1989).
30. S. I. Prokofjev, Def. Diff. Forum **194–199**, 1141 (2001).
31. B. B. Straumal, S. A. Polyakov, and E. J. Mittemeijer, Acta Mater. **54**, 167 (2006).
32. G. Gottstein and L. S. Shvindlerman, *Grain Boundary Migration in Metals* (CRC, Boca Raton, 1999).

33. B. B. Straumal, V. G. Sursaeva, and L. S. Shvindlerman, *Fiz. Met. Metalloved.* **49**, 1021 (1980) [Phys. Met. Metall. **49**, 102 (1980)].
34. U. Czubayko, V. G. Sursaeva, G. Gottstein, and L. S. Shvindlerman, *Acta Mater.* **46**, 5863 (1998).
35. M. V. Klassen-Neklyudova, *Mechanical Twinning of Crystals* (Akad. Nauk SSSR, Moscow, 1960; Consultants Bureau, New York, 1964).
36. V. G. Sursaeva, U. Czubayko, G. Gottstein, and L. S. Shvindlerman, *Mater. Sci. Forum* **294–296**, 517 (1999).
37. A. U. Tuflin, V. G. Sursaeva, and U. Czubayko, *Defect Diff. Forum* **194–199**, 1253 (2001).
38. B. B. Straumal and L. S. Shvindlerman, *Acta Metall.* **33**, 1735 (1985).
39. B. B. Straumal and L. S. Shvindlerman, *Poverkhnost'*, No. 10, 5 (1986) [in Russian].
40. E. L. Maksimova, B. B. Straumal, and L. S. Shvindlerman, *Fiz. Tverd. Tela (Leningrad)* **28**, 3059 (1986) [Sov. Phys. Solid State **28**, 1721 (1986)].
41. E. L. Maksimova, B. B. Straumal, and L. S. Shvindlerman, *Fiz. Met. Metalloved.* **63**, 885 (1987) [Phys. Met. Metall. **63**, 45 (1987)].
42. E. L. Maksimova, E. I. Rabkin, B. B. Straumal, and L. S. Shvindlerman, *Fiz. Met. Metalloved.* **64**, 511 (1987) [Phys. Met. Metall. **64**, 87 (1987)].
43. E. L. Maksimova, L. S. Shvindlerman, and B. B. Straumal, *Acta Metall.* **36**, 1573 (1988).
44. E. L. Maksimova, E. I. Rabkin, L. S. Shvindlerman, and B. B. Straumal, *Acta Metall.* **37**, 1995 (1989).
45. E. L. Maksimova, B. B. Straumal, and L. S. Shvindlerman, *Fiz. Met. Metalloved.* **67**, 959 (1989) [Phys. Met. Metall. **673**, 123 (1989)].
46. E. L. Maksimova, L. S. Shvindlerman, and B. B. Straumal, *Acta Metall.* **37**, 2855 (1989).
47. E. L. Maksimova, E. I. Rabkin, L. S. Shvindlerman, and B. B. Straumal, *Def. Diff. Forum* **66–69**, 869 (1990).
48. K. Shin and A. H. King, *Philos. Mag. A* **63**, 1023 (1991).
49. F.-R. Chen and A. H. King, *Acta Crystallogr. B* **43**, 416 (1987).
50. B. B. Straumal, S. A. Polyakov, E. Bischoff, et al., *Interface Sci.* **9**, 287 (2001).
51. B. B. Straumal, V. G. Sursaeva, and S. A. Polyakov, *Interface Sci.* **9**, 275 (2001).
52. W. Krakow and D. A. Smith, *Ultramicroscopy* **22**, 47 (1987).
53. F. Ernst, M. W. Finnis, D. Hoffmann, et al., *Phys. Rev. Lett.* **69**, 620 (1992).
54. T. Watanabe, S.-I. Kimura, and S. Karasima, *Philos. Mag. A* **49**, 845 (1984).
55. B. B. Straumal, V. G. Sursaeva, and A. S. Gornakova, *Z. Metallkund.* **96**, 1147 (2005).
56. B. B. Straumal, A. S. Gornakova, and V. G. Sursaeva, *Philos. Mag. Lett.* **88**, 27 (2008).

*Translated by Yu. Sin'kov*